

1988

A Computer Model for Scroll Compressors

Jean-Luc Caillat
Copeland Corporation

Shimao Ni
Copeland Corporation

Michael Daniels
Copeland Corporation

Follow this and additional works at: <http://docs.lib.purdue.edu/icec>

Caillat, Jean-Luc; Ni, Shimao; and Daniels, Michael, "A Computer Model for Scroll Compressors " (1988). *International Compressor Engineering Conference*. Paper 601.
<http://docs.lib.purdue.edu/icec/601>

This document has been made available through Purdue e-Pubs, a service of the Purdue University Libraries. Please contact epubs@purdue.edu for additional information.

Complete proceedings may be acquired in print and on CD-ROM directly from the Ray W. Herrick Laboratories at <https://engineering.purdue.edu/Herrick/Events/orderlit.html>

A COMPUTER MODEL FOR SCROLL COMPRESSORS

Jean-Luc Caillat
Manager-Research

Shimao Ni
Sr. Project Eng

Michael Daniels
Project Engineer

Research and Development Department
Copeland Corporation
Sidney, Ohio, USA

INTRODUCTION

The growing need for higher efficiency, superior reliability, low cost compressors, and the inherent opportunity for a competitive edge have motivated the manufacturers to develop state-of-the-art analytical tools to predict, evaluate, and optimize the performance of new designs.

Over the years, a considerable number of such tools have been the subject of papers presented at the International Compressor Engineering Conference at Purdue; a few of which have been devoted to the overall performance simulation of reciprocating, rotary, and screw type compressors.

The following real time global model was developed to analyze geometric, dynamic, thermodynamic, and heat transfer characteristics of scroll compressors for a variety of conditions and applications. The general organization of the simulation is shown in Figure 1.

1. The compression process was simulated for every gas pocket, irrespective of their number and dimensions, along with interpocket fluid leakage.
2. The discharge process model capabilities included various vane geometries and porting configurations for enhanced versatility.
3. The pertinent forces and moments, including coulombic and hydrodynamic frictional effects, were evaluated to derive the overall shaft power requirement.
4. A simple motor model was incorporated to allow both single and variable-speed analyses.
5. Finally an overall energy balance, incorporating heat transfer effects, was performed iteratively. This resulted in mass flow, capacity, input power, and ultimately overall efficiency predictions.

THERMOFLUID MODEL

The compression process is illustrated in Figure 2. Compression initiates with the closing of the suction pocket. This compression pocket then undergoes a reduction in volume. When the vanes can no longer separate this pocket from the central volume, it is designated an adjacent central volume. Upon pressure equalization between these volumes, the distinction between them vanishes and the compression process is concluded. Additionally, a discharge process takes place between the central volume and an isobaric plenum.

Assumptions

The thermofluid model depended upon several assumptions for a workable analysis. They may be summarized as follows:

1. Due to the symmetry of scrolls, only one compression path was evaluated. Properties along the other compression path were considered identical.
2. Mass flows calculated on a differential basis were assumed constant during the time period considered.

Other more specific assumptions are stated in the model's description

that follows.

Geometrical Calculations

Geometrical parameters such as volumes and areas provided the basis for the positive displacement analysis. For involute type vanes, base areas of each compression pocket [1] were evaluated using:

$$S = 1/2 \int_{\theta'}^{\theta'+2\pi} (R_g \theta) (R_g \theta d\theta) \quad (1)$$

The product of each of these areas with vane height yielded the volume of each compression pocket. The evaluation of interpocket leakage requires the average vane length separating each pocket from one another. This leakage path length [1] was determined by the following:

$$L = \int_{\theta'}^{\theta'+2\pi} R_g \theta d\theta \quad (2)$$

The central volume was also evaluated with various inner vane geometries and porting configurations considered. These calculations, although rudimentary, are lengthy and will be avoided here. Two points of this evaluation, however, are of special interest. The adjacent central volume opening up to the central volume was modeled as two volumes separated by a converging nozzle. The throat was chosen at the minimum distance between the separating flanks. Volumes were then calculated appropriately. The discharge hole opening was determined taking into account any occlusion due to the orbiting vane.

Compression Process

The compression process was modeled using two distinct processes: an isentropic compression and an interpocket leakage. The simplification was to let these processes occur independently and consecutively. Crank steps of five degrees or less yielded consistent results, thus justifying this simplification.

The first step was to model the compression as isentropic. Specific volume was determined exclusively by the change in volume of the compression pocket. These two properties were sufficient to fix the state. Remaining real gas properties were then determined.

The interpocket leakage processes are illustrated in Figure 3. For any particular pocket, two discrete leakage mechanisms exist; paths are between tips and bases and sealing portions of vane flanks. A combination of constant and thermally dependent clearances were used.

Considering only the leakage between the tips and bases, flow rates that include frictional effects [2] were determined using:

$$\dot{m} = A_{bt} \sqrt{2 \Delta P \rho_u D_h / (fL)} \quad (3)$$

Iteration was required since the friction factor, f , is dependent on Reynold's number, which in turn is dependent upon mass flow.

Flank leakage was modeled as a converging nozzle. With a known pressure difference and flank clearance, an assumption of isentropic steady-state compressible flow [3] yields:

$$\dot{m} = kA_f \sqrt{P_u \rho_u 2/(\gamma-1) (R_p^{2/\gamma} - R_p^{(\gamma+1)/\gamma})} \quad (4)$$

Pressure ratios were limited between no flow and choked flow conditions:

$$1 > R_p > \left[\frac{2}{\gamma + 1} \right] \gamma / (\gamma - 1) \quad (5)$$

After determining interpocket mass flows, energy and mass balances provided the internal energy and specific volume, respectively, of each pocket. The states were fixed, and other real gas properties were readily determined.

Due to the comparatively smaller flow area, flank leakage was usually the weaker mechanism. However, when an adjacent central volume existed, much larger flank leakage resulted. Due to the transient nature of this process (both in flank separation and pressure differences), diminished crank increments of one half of a degree were required. As stated earlier, when pressures equalized between these two volumes, no further distinctions between the two volumes were made. This marked the conclusion of the compression process.

Discharge Process

The plenum was assumed to be sufficiently large to allow for constant properties of state. Flows between the central volume and discharge plenum were determined using the Bernoulli Equation [2]:

$$\dot{m} = A_d \sqrt{2\Delta P \rho_u} \quad (6)$$

Additionally, an energy balance and mass balance were performed on the central volume. An iterative technique determined a mass flow that satisfied both the energy and Bernoulli constraints. Internal energy and specific volume fixed the state, and other real gas properties were determined.

Plenum conditions were determined by summing the total energy and mass leaving the central volume during an entire revolution. This internal energy, coupled with the known condensing pressure, fixed the state. Plenum conditions, therefore, were updated every revolution. The initially assumed discharge state thus required several revolutions before convergence to steady-state discharge conditions.

DYNAMIC ANALYSIS

The program calculated various forces involved in the compressor dynamics. Considering an axially and radially compliant scroll compressor, these forces included:

1. Axial, radial and tangential forces acting on the tips, bases, and vane flanks.
2. Balancing forces sealing the fixed scroll axially and radially with the orbiting scroll.
3. Inertial forces of unbalanced masses such as orbiting scroll, counterweights, and oldham ring.
4. Friction forces between various moving components, such as vane flanks, vane tips and bases, thrust bearing members, and journal bearings.
5. Reaction forces on the shaft and journal bearings.

The corresponding moments were evaluated from these forces and the geometrical dimensions of the compressor. Hence, the overall shaft power, torque, and motor power requirements were computed.

In the compression process modeling, all the geometric and thermodynamic parameters of gas pockets; i.e., areas, volumes, pressures, temperatures, and specific volumes were previously evaluated for every crank angle. Thus the gas forces acting on the tips, bases and flanks of scroll vane and their radial, tangential, and axial components were readily calculated.

The gas forces that tend to separate the mating scrolls axially

and radially, were balanced. The real time global compressor model having the capability to optimize the balancing scheme calculated the required balancing forces.

The scroll compressor rotating at high speed requires accurate inertial force balance to reduce vibration and noise. The inertial force of the orbiting scroll and the oldham ring, etc., were balanced by assigned counterweights.

Two types of friction were considered in the scroll model: coulombic and hydrodynamic. The coulombic friction was assumed to take place where boundary type lubrication occurs, such as in scroll vane tip-base and flank-flank sliding contact. The numerical value of the coulombic friction coefficient was determined by experiments and correlated with the recommendation of a Mechanical Engineering handbook [2]. The hydrodynamic friction takes place between lubricated surfaces developing adequate oil films; i.e., journal bearings and thrust surfaces. For the thrust bearing, the magnitude of the hydrodynamic friction force was calculated using the following expression:

$$F_f = V\mu A_t/t \quad (7)$$

It was assumed in Eq. (7) that the oil film thickness is directly proportional to the load. Experimental measurements were performed to obtain the proportionality relations for specific loading of given thrust bearings. The friction torque in the journal bearings were calculated in a bearing subroutine. This subroutine analyzes design parameters of journal bearings by use of the Mobility method for dynamically loaded journal bearings [4]. The curve fitting equations for mobility calculations were based on Finite Element Analysis of journal bearings [5]. An iteration scheme was used to obtain a periodic locus of the shaft center under dynamic loads yielding the oil film thickness at every crank angle. Thus the friction torque was calculated considering average mass flow rate and temperature of the lubricants. Also the minimum oil film thickness and the associated maximum pressure and location were computed.

The bearing calculations require the knowledge of loads including friction effects which are dependent upon those loads. Hence an iteration scheme was used to obtain the solution of the overall forces and moments balance.

After all pertinent forces and moments involved in the dynamics of the scroll compressor were calculated, the overall shaft torque was readily evaluated. A subroutine, using the motor torque-speed-efficiency relationships, provided the motor efficiency and updated the motor speed necessary for all the calculations above. Using the new motor speed, the previous procedure was then repeated until the motor speed converged. By the use of this iteration scheme, consistency among motor speed, efficiency, torque output, and power requirements was obtained.

ENERGY BALANCE

The purpose of the energy balance is to determine the gas internal superheat which in turn allows to calculate the inlet gas temperature, density, mass flow rate, and compressor capacity. The overall energy balance model is shown in Figure 4. In the program the internal superheat was calculated through an iteration scheme shown in Figure 5.

As shown in Figure 4, the total electric power input to the motor was divided into two parts: the motor loss and the mechanical shaft work. The latter consisted of the gas compression work and all mechanical friction losses. The heat generated by the motor loss, the mechanical friction, and the heat transferred by the discharge gas to the compressor were merged into a fictitious internal heat source. At

steady-state the output from this heat source was partitioned into the internal superheat absorbed by the return gas, before it enters the scroll inlet pockets, and the heat exchanged by the shell to the ambient. A semi-empirical block heat transfer model was developed to simulate the energy transport process, including all internal and external conduction, convection, and radiation heat transfer. The internal superheat was taken as a function of the discharge temperature and the operating condition, such as the condensing and evaporating temperatures. The heat dissipated to the ambient through convection and radiation heat transfer was evaluated as a function of the temperatures of the shell and the ambient. The internal superheat was initially assumed to be zero. As a result of the overall energy balance, a new internal superheat was calculated. Equilibrium was reached due to the shell heat dissipation, and both the suction and the discharge temperatures converged.

RESULTS

Scroll compressor performance was predicted for a given design at various operating pressure conditions and constant speed. As a benchmark test to the comprehensive computer simulation, the results were compared with actual scroll compressor test data for capacity and EER. These comparisons are shown in Figures 6 and 7.

The predicted capacities shown in Figure 6 are in excellent agreement with the experimental data over a wide range of operating conditions. This agreement demonstrates the validity of the leakage, gas compression, and energy balance models incorporated in the simulation. Generally good agreement in EER is shown in Figure 7. However, predicted EER is lower at higher condensing temperature and conversely higher at lower condensing temperature.

The simulation was extended to air conditioning and heat pump variable speed applications. The comparison of predicted EER with test data is shown in Figure 8. The results are generally in good agreement. However, slight deviations were observed at low evaporating temperature and high speed.

The authors believe these slight discrepancies can be reduced by improving the current friction and motor models.

CONCLUSION

An overview of the overall computer simulation for scroll compressors has been presented. The results, while pointing to some potential areas of improvement, show good agreement between simulation predictions and measurements performed under various conditions. The general validation of the model and its value have been confirmed as a valuable tool in the optimization of scroll compressor design.

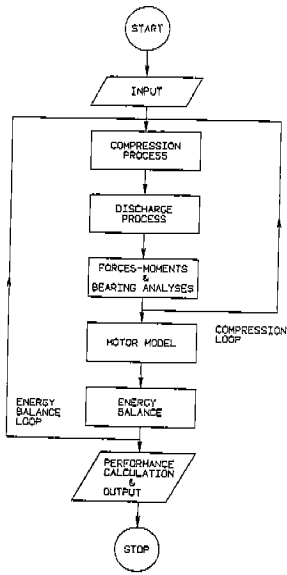
NOMENCLATURE

A_d	=	flow area of discharge passage
A_f	=	leakage flow area between vane flank surfaces
A_{bt}	=	leakage flow area between tips and bases
A_t	=	thrust bearing area
D_h	=	hydraulic diameter
F_f	=	friction force
f	=	friction factor - Moody
k	=	contraction coefficient - empirical
L	=	interpocket tip/base leakage path length
\dot{m}	=	mass flow rate = $dm/d(\text{time})$
P_u	=	upstream pressure
R_g	=	involute generating radius
R_p	=	downstream to upstream pressure ratio
S	=	compression pocket base area
t	=	oil film thickness
V	=	relative velocity

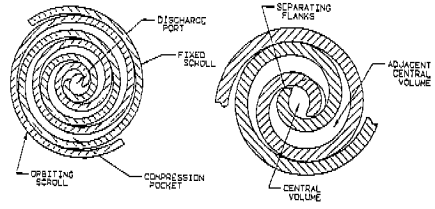
T_{rg} = return gas temperature
 T_s = scroll inlet temperature
 T_{snew} = updated scroll inlet temperature
 σ = isentropic expansion coefficient
 ΔP = interpocket pressure difference
 ΔT_s = internal superheat
 Σ = convergence criterium
 θ'_i = sealed pocket angle
 ρ_u = upstream density
 μ = dynamic viscosity

REFERENCES

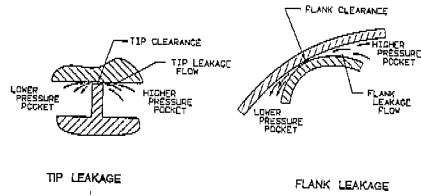
- [1] Caillat, J-L., Scroll Report, Copeland Internal Report, 1981
- [2] Marks' Standard Handbook of Mechanical Engineering, Eighth Edition, McGraw Hill.
- [3] Zucrow, M. J. and Hoffman, J. D., Gas Dynamics, Vol. 1, Wiley, 1976.
- [4] Booker, J.F., "Dynamically Loaded Journal Bearings: Numerical Application of the Mobility Method", Trans. ASME, Journal of Lubrication Technology, Vol. 93, January 1971, pp. 168-178. Errata: No. 2, April 1971, p. 315.
- [5] Goenka, P.K., "Analytical Curve Fits for Solution Parameters of Dynamically Loaded Journal Bearings", Journal of Tribology, Vol. 106, Oct. 1984, pp. 421-428.



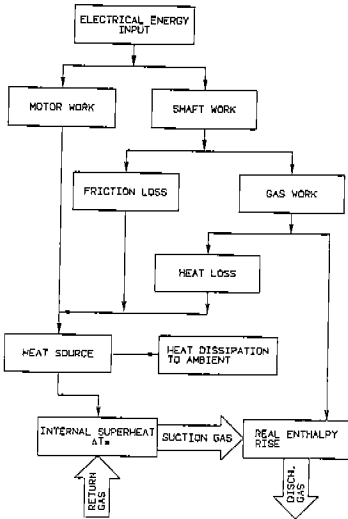
ORGANIZATION OF SIMULATION
FIGURE 1



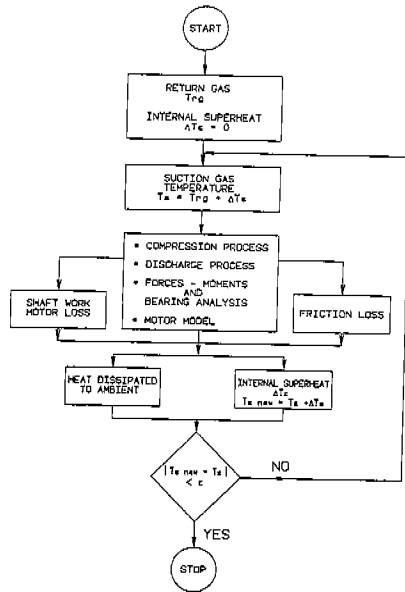
COMPRESSION PROCESS ILLUSTRATION
FIGURE 2



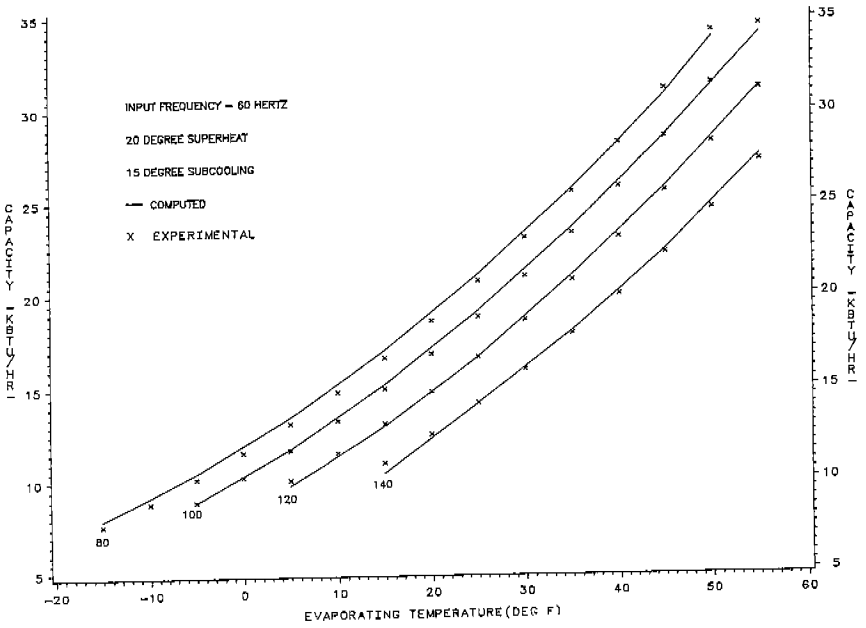
LEAKAGE PATHS ILLUSTRATION
FIGURE 3



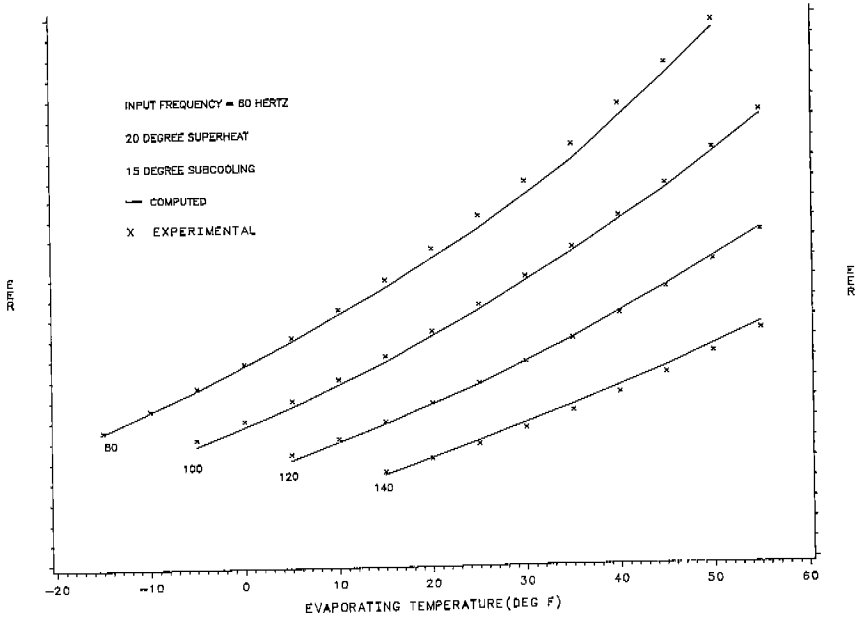
ENERGY BALANCE MODEL
FIGURE 4



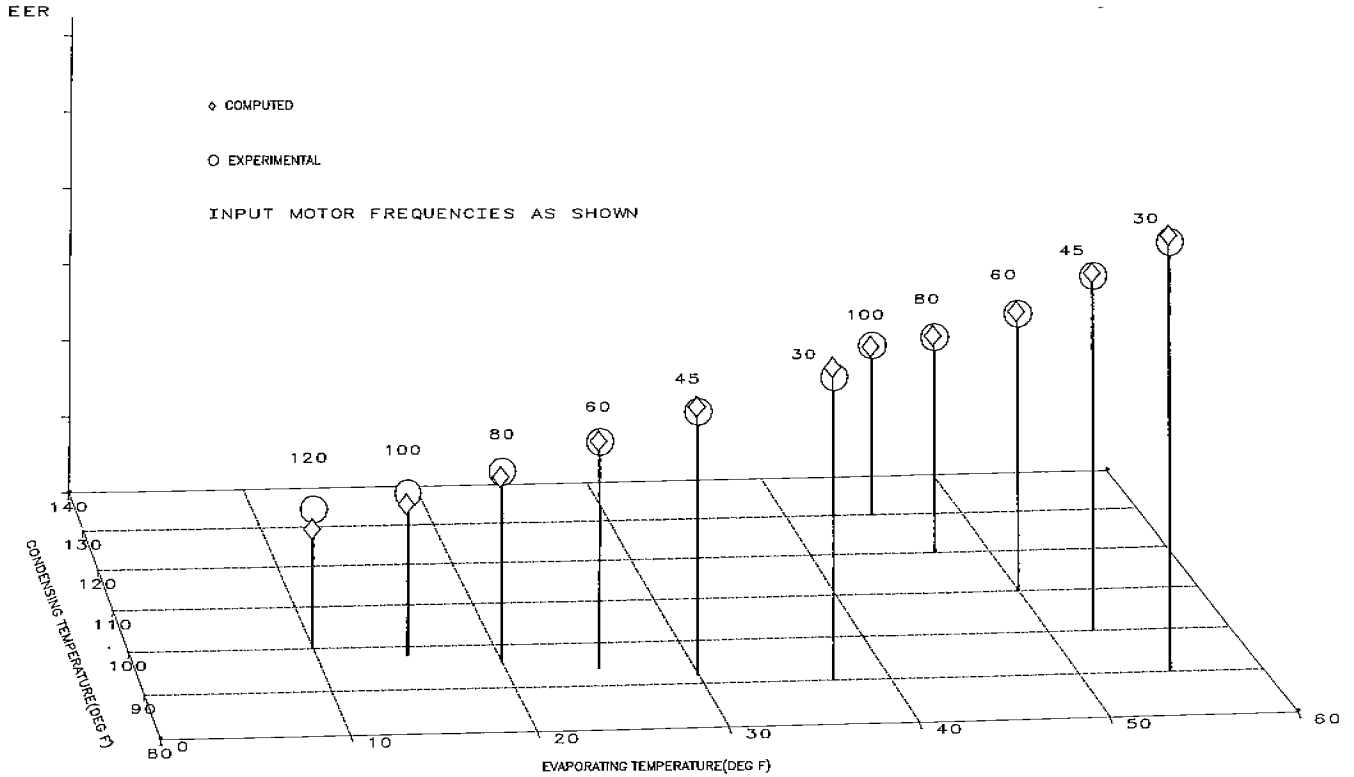
ENERGY BALANCE ITERATIVE SCHEME
FIGURE 5



CAPACITY COMPARISON AT VARIOUS EVAPORATING AND CONDENSING TEMPERATURES
 FIGURE 6



EER COMPARISON AT VARIOUS EVAPORATING AND CONDENSING TEMPERATURES
 FIGURE 7



EER COMPARISON FOR VARIABLE SPEED AIR CONDITIONING AND HEAT PUMP APPLICATIONS

FIGURE 8